On the propagation of low-frequency fluctuations in the plasma sheet: 1, CLUSTER observations and magnetohydrodynamic analysis.

P. Louarn, G. Fruit, E. Budnik, J.A. Sauvaud, C. Jacquey, D. Le Quéau, H. Rème, E. Lucek, A. Balogh

On the propagation of low-frequency fluctuations in the plasma sheet: 1. Cluster observations and magnetohydrodynamic analysis

P. Louarn,[1] G. Fruit,[2] E. Budnik,[1] J. A. Sauvaud,[1] C. Jacquey,[1] D. Le Quéau,[1] H. Rème,[1] E. Lucek,[3] and A. Balogh[3]

Received 9 September 2003; revised 22 December 2003; accepted 22 January 2004; published 24 March 2004.

[1] Low-frequency pressure and magnetic oscillations observed by Cluster in the plasma sheet are investigated with the aim of determining if they are magnetohydrodynamic (MHD) eigenmodes. We analyze the plasma sheet crossing occurring on 22 August 2001, as the magnetosphere was first quiet and then active, and compare the observations with theoretical results concerning the MHD propagation in a Harris sheet. The theory shows that the eigenmodes have periods scaled by a characteristic time, τ, equal to the ratio between (1) the thickness of the sheet and (2) the sound speed. Using the Cluster 4 spacecraft, we estimate the sheet thickness and determine this characteristic time. It is compared with the typical periods of the fluctuations deduced from a wavelet analysis. During the quiet period, the fluctuations have periods larger than 100 s or 15τ. Discrete MHD eigenmodes with such periods would have wavelengths larger than the distance separating Cluster from Earth (18 R_E). Thus they are very unlikely interpreted as freely propagating eigenmodes. However, fluctuations of shorter periods ($\sim$20 s) are observed during and just after the substorm onset. We demonstrate that they are compatible with the fundamental MHD eigenmode (kink-like mode) of the sheet, with a wavelength of $\sim$5–6 R_E, their direction of propagation being not determined at this stage of the analysis. We thus conclude that freely propagating MHD eigenmodes observable by Cluster would have periods that hardly exceed a minute for typical plasma sheet parameters (thickness of 1 R_E, temperature of a few keV). *INDEX TERMS:* 2744 Magnetospheric Physics: Magnetotail; 2752 Magnetospheric Physics: MHD waves and instabilities; 2764 Magnetospheric Physics: Plasma sheet; 2788 Magnetospheric Physics: Storms and substorms; *KEYWORDS:* magnetotail, MHD waves and instabilities, plasma sheet, storms and substorms

Citation: Louarn, P., G. Fruit, E. Budnik, J. A. Sauvaud, C. Jacquey, D. Le Quéau, H. Rème, E. Lucek, and A. Balogh (2004), On the propagation of low-frequency fluctuations in the plasma sheet: 1. Cluster observations and magnetohydrodynamic analysis, *J. Geophys. Res.*, *109*, A03216, doi:10.1029/2003JA010228.

1. Introduction

[2] The understanding of the dynamics of current sheets is a preeminent problem of space physics. Current sheets pervade space plasmas; they present a very dynamical behavior that may lead to phenomena as impressive as solar eruptions and magnetospheric substorms. Their thinning favors the development of still not fully explained processes that often trigger spectacular evolutions of the magnetic field topology and accelerate particles. Current sheets also support the propagation of linear fluctuations. These waves can dissipate a part of the electric current and thus can contribute to the magnetic topology evolutions. From a theoretical point of view, their study is the first step before analyzing nonlinear phenomena. Moreover, as any investigations of the linear response of a physical system, it provides a wealth of information on the organization and the dynamics of the system itself.

[3] Waves with periods from a fraction of second to a few tens of minutes have been observed in the Earth's magnetotail down to the Earth's surface (see *Patel* [1968], *Siscoe* [1969], and *McKenzie* [1970] for early works on the subject). As proposed by various theoretical analysis, a large variety of perturbations could propagate in current sheets, with potential energetic and/or structural consequences on the equilibrium of the sheet. One may quote the classical MHD oscillations [*Seboldt*, 1990; *Smith et al.*, 1997; *Tirry et al.*, 1997; *Fruit et al.*, 2002a], the different forms of tearing [see, e.g., *Coppi et al.*, 1966; *Schindler and*

[1]Centre d'Etude Spatiale des Rayonnements, Toulouse, France.
[2]Department of Mathematics, University of Waikato, Hamilton, New Zealand.
[3]Imperial College, London, UK.

0148-0227/04/2003JA010228

Ness, 1974; *Lembege and Pellat*, 1982; *Coroniti*, 1985; *Lee et al.*, 1988; *Pellat et al.*, 1991; *Pritchett*, 2001, and references therein], the lower hybrid drift instability [*Krall and Liewer*, 1971; *Huba et al.*, 1980], the cross-field streaming instability [*Lui*, 1996], the ion-Weibel instability, the ballooning instability [*Miura et al.*, 1989; *Roux et al.*, 1991], and the kinetic drift-kink instability [*Lapenta and Brackbill*, 1997; *Daughton*, 1998, 2002]. These different types of waves may coexist in the sheet. They may be relatively simple forms of MHD and bifluid fluctuations or may be related to more complex kinetic processes. They may also correspond to the development of instabilities in the sheet or be a part of the linear stable response of the sheet to external perturbations. Their observational identification will certainly greatly help to understand the current sheet dynamics. Along this line, *Bauer et al.* [1995a, 1995b] have analyzed compressional neutral sheet oscillations with AMPTE, demonstrating that they are particularly powerful at substorm onsets. These analysis are also related to an important aspect of substorm physics: the identification of the generation mechanisms of Pi2 oscillations [see *Kepko and Kivelson*, 1999]. It is in this general framework that we analyze the low-frequency fluctuations observed in the plasma sheet by Cluster.

[4] In homogeneous media the mode identification is performed directly in the spatial/temporal ($\vec{k}$, ω) Fourier space both experimentally and theoretically. However, current sheets being nonhomogeneous, the investigation is more complex and a simple Fourier analysis is not sufficient. The characteristics of the fluctuations, as their polarization, depend on space. The structure of the eigenmodes must be determined in the whole space and the position of the observer must be precisely known before interpreting the observations. Multispacecraft observations, as Cluster ones, are then crucial.

[5] We consider here the linear MHD theory and apply the results of the theoretical analysis performed by *Fruit et al.* [2002a, 2002b]. The current sheet is supposed to be a one-dimensional (1-D) Harris sheet [*Harris*, 1962] which is an exact 1-D solution of both the MHD and the kinetic Vlassov-Maxwell equations. It is known that a Harris sheet is stable to ideal MHD instabilities [*Dahlburg et al.*, 1992] but unstable to a number of nonideal and kinetic instabilities. As shown by *Fruit et al.* [2002a, 2002b], this 1-D structure is sufficiently simple to perform a complete analysis of the linear MHD response of the system to different forms of excitations. By comparing the ideal MHD results and the observations, it is possible to distinguish oscillations that are simple stable MHD eigenmodes (that exist in any case if the sheet is externally perturbed) from internal instabilities. In the present paper, we perform a temporal analysis of Cluster data. By comparing the timescale of the fluctuations with the characteristic MHD timescale of the sheet, we identify possible MHD eigenmodes. The detail of the signal reconstruction, including the quantitative estimates of the amplitude of the perturbations and the decomposition into sausage and kink oscillations, will be performed in a companion paper [*Fruit et al.*, 2004].

[6] In section 2 we summarize the main theoretical results. In section 3 we analyze the crossing of the plasma sheet occurring on 22 August 2001, and we determine the characteristic length and timescales of the MHD eigenmodes using the four spacecraft measurements. This event was also studied by *Volwerk et al.* [2003], who identified a long period kink-like oscillation without, nevertheless, an explicit comparison with the MHD theory. In section 4 we use a wavelet analysis to estimate the typical timescales of the fluctuations and compare them with the MHD characteristic time. The results are discussed in section 5.

2. MHD Propagation in a Harris Sheet: Characteristic Times and Lengths

[7] Detailed discussions concerning the MHD propagation in the plasma sheet and the magnetotail can be found in the works of *Seboldt* [1990], *Smith et al.* [1997], and *Tirry et al.* [1997]. These studies investigate the solutions of the ordinary differential equation that describes the spatial variations of the MHD modes in the direction of nonhomogeneity. The determination of the spectral characteristics of the Fourier modes is a first step in the theoretical analysis that, as shown here, already offers many opportunities for comparison with Cluster data and may lead to the identification of possible MHD-type perturbations. The next steps consist in the determination of the Green function of the system, in its excitation by realistic external perturbation and, finally, in the reconstruction of the corresponding spatial-temporal perturbation [see *Fruit et al.*, 2002a, 2002b]. This complete theoretical analysis and the comparison with the MHD-type oscillations that are identified here will be considered in the companion paper [*Fruit et al.*, 2004].

2.1. Equilibrium, Boundary Conditions, and Basic Equations

[8] The sheet is described by the Harris equilibrium characterized by:

$$B_{eq}(z) = -B_e \tanh\left(\frac{z}{a}\right), \tag{1}$$

$$\rho_{eq}(z) = \rho_e \tanh^2\left(\frac{z}{a}\right) + \frac{\rho_0}{\cosh^2\left(\frac{z}{a}\right)}. \tag{2}$$

We will use normalized variables: (1) the half-thickness of the plasma sheet (a) will scale the distances, (2) the magnetic field and the density will be normalized to their values in the lobes, (3) the different speeds will be normalized to the sound velocity v_s and, (4) time will be normalized to $\tau = a/v_s$, the characteristic MHD time. a and τ are two fundamental parameters of the study that will be estimated using the four -spacecraft capabilities of Cluster. From the standard equations of ideal MHD with a polytropic pressure law and using a Fourier transform in the x and y directions and in time, one gets a differential equation for the transversal displacement field $\hat{\xi}_z$ (see details in the work of *Seboldt*, [1990]):

$$\frac{d}{dz}\left[f_{\omega,k_x,k_y}(z)\frac{d\hat{\xi}_z}{dz}\right] + g_{\omega,k_x,k_y}(z)\hat{\xi}_z = 0, \tag{3}$$

with

$$f_{\omega,k_x,k_y}(z) = \rho_{eq}(z)\left(v_s^2 + v_A^2\right) \times \frac{\left(\omega^2 - k_x^2 v_A^2\right)\left(\omega^2 - k_x^2 v_c^2\right)}{\left(\omega^2 - \omega_+^2\right)\left(\omega^2 - \omega_-^2\right)}, \quad (4)$$

$$g_{\omega,k_x,k_y}(z) = \rho_{eq}(z)\left(\omega^2 - k_x^2 v_A^2\right). \quad (5)$$

and

$$\omega_\pm^2 = \frac{1}{2}\left(k_x^2 + k_y^2\right)\left(v_s^2 + v_A^2\right) \times \left[1 \pm \sqrt{1 - 4\frac{k_x^2}{k_x^2 + k_y^2}\frac{v_s^2 v_A^2}{\left(v_s^2 + v_A^2\right)^2}}\right] \quad (6)$$

In these equations, $v_A = \sqrt{B_{eq}^2/\left(\mu_0 \rho_{eq}\right)}$ is the Alfven speed and $v_c = \sqrt{v_A^2 v_s^2/\left(v_A^2 + v_s^2\right)}$ the cusp velocity.

[9] Equation (3) is a second-order differential equation of the standard Sturm-Liouville type. It becomes singular if $f(z)$ reaches zero, that is, whenever the phase speed of the wave matches the Alfven or the cusp velocities. As discussed in a number of papers, the existence of such a singularity leads to a continuous spectrum of eigensolutions, which diverge logarithmically at the singular point [see, e.g., *Fruit et al.*, 2002b]. Here we restrict the analysis to the discrete modes only, thus to the regular solutions of equation (3).

[10] In order to integrate equation (3), the boundary conditions in z have to be specified. For given values of ω and k_x, k_y, f, and g are functions of z only. They become constant for large value of z (f_e and g_e, respectively) and the equation (3) becomes $f_e \hat{\xi}_z'' + g_e \hat{\xi}_z = 0$. The solutions of this simple second-order differential equation depend on the sign of

$$\alpha_e^2 = -\frac{g_e}{f_e} = -\frac{\left(\omega^2 - \omega_{+e}^2\right)\left(\omega^2 - \omega_{-e}^2\right)}{\left(v_s^2 + v_{Ae}^2\right)\left(\omega^2 - k_x^2 v_{ce}^2\right)}. \quad (7)$$

[11] In the frequency domain where $\alpha_e^2 < 0$, the solution is sinusoidal far from the neutral sheet and corresponds to waves propagating towards the free space. It means that a local deposition of energy near $z = 0$ will spread throughout the whole space. The corresponding solutions are thus expected to play a minor role in the perturbations of the neutral sheet observed far from the initial pressure pulse. On the other hand, when $\alpha_e^2 > 0$ the solutions are localized waves or surface modes. In that case the deposited energy remains within the sheet and the relating solutions will dominate the neutral sheet perturbations. When $\omega < k_x v_{Ae}$ or $\omega < k_x v_{ce}$, there exists some point z_s in the current sheet where f is null. In these frequency domains, equation (3) has singular solutions that we discard here. We thus consider the (ω, k_x, k_y) space domains where the coefficient α_e^2 is positive. It is shown in Figure 1 for particular values of k_x and k_y. If $k_y = 0$ (upper diagram), the Alfven continuum disappears and only the cusp continuum remains below the $\omega = k_x v_{ce}$ line (crosshatched domain). The interesting domain lies thus between the lines $\omega = k_x v_s$ and $\omega = k_x v_{Ae}$.

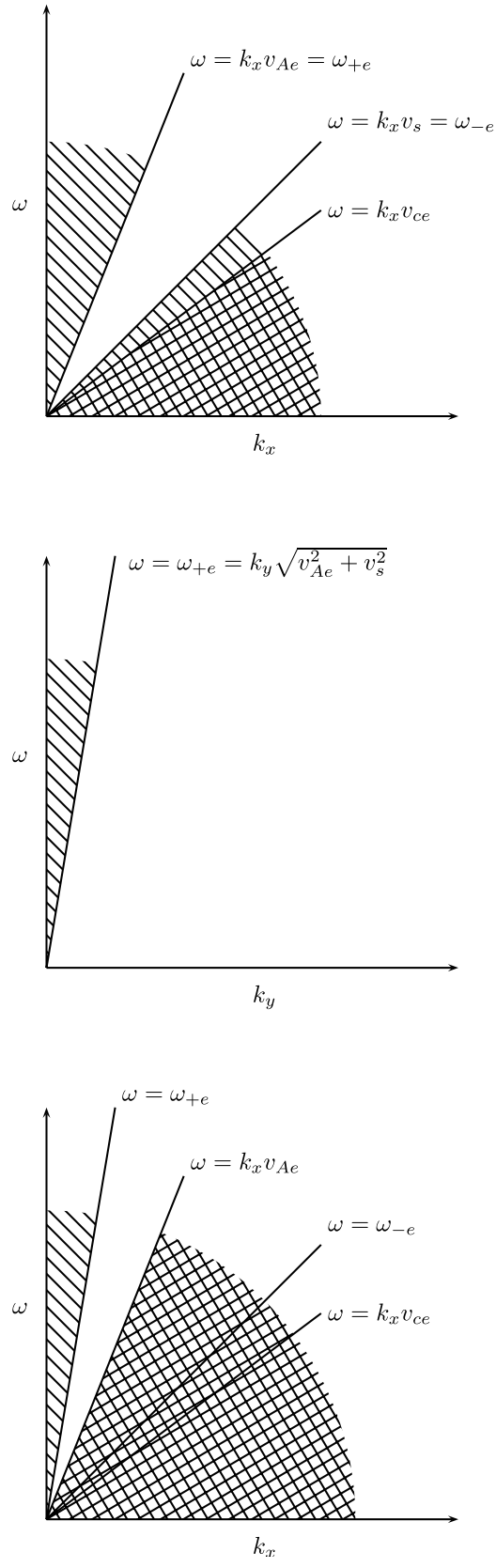

Figure 1. Nature of the modes in (ω, k_x, k_y) diagrams, from the top: (a) pure parallel propagation ($k_y = 0$), (b) pure transverse propagation ($k_x = 0$), (c) oblique propagation ($k_x = k_y$). The simple hatched domains correspond to the radiating modes The double hatched domains corresponds to the continuum (Alfven or cusp). The relevant domains for the present analysis are left in white.

This case was thoroughly studied by *Fruit et al.* [2002a]. If $k_x = 0$ (central diagram) the two continua collapse and equation (3) becomes completely regular: the relevant region lies below the $\omega = k_y\sqrt{v_{Ae}^2 + v_s^2}$ line. Finally, for $k_x \neq 0$ and $k_y \neq 0$ (lower diagram), the domain of interest is between the lines $\omega = k_x v_{Ae}$ and $\omega = \omega_{+e}$. Hence in these regions of the dispersion diagram where $\alpha_e^2 > 0$, the solution of equation (3) takes the simple form: $\hat{\xi}_z = A \pm \exp(-\alpha_e|z|)$ far from the neutral sheet (at $|z| \geq l \gg a$). The matching conditions at $z = \pm l$ are thus the continuity of the displacement $\hat{\xi}_z$ and of the total pressure, related to the quantity $f\hat{\xi}'_z$. The required boundary conditions read simply: $\hat{\xi}'_z = \mp \alpha_e \hat{\xi}_z$ for $z = \pm l$. The problem to solve is therefore written as:

$$\begin{aligned} \frac{d}{dz}\left[f_{\omega,k_x,k_y}(z)\frac{d\hat{\xi}_z}{dz}\right] + g_{\omega,k_x,k_y}(z)\hat{\xi}_z &= 0 \\ \hat{\xi}'_z(l) + \alpha_e\hat{\xi}_z(l) &= 0 \\ \hat{\xi}'_z(-l) - \alpha_e\hat{\xi}_z(-l) &= 0, \end{aligned} \tag{8}$$

where l is large compared with a, such that the three coefficients are almost constant beyond. Let us note finally that the coefficients in equation (3) are symmetric, as well as the boundary conditions, so that the problem in equation (8) has either symmetric or antisymmetric solutions.

2.2. Dispersion Relations

[12] The problem in equation (8) is numerically solved using a fourth-order Runge-Kutta procedure for fixed values of k_x and k_y, starting from $z = 0$ with $\hat{\xi}_z = 0$ for antisymmetric modes and $\hat{\xi}'_z = 0$ for symmetric ones with a test value ω. The eigenvalue ω is changed whenever the boundary condition at $z = l = 10\,a$ is not satisfied. We thus obtain a discrete set of eigenvalues $\omega_n(k_x, k_y)$ and eigenfunctions $\psi_n(z)$ representing the global modes of the Harris sheet. The integer n corresponds to the number of nodes in the spatial eigenfunction ψ_n.

[13] Two limited cases will be analyzed here: pure parallel propagation ($k_x \neq 0$ and $k_y = 0$) and pure transverse propagation ($k_x = 0$ and $k_y \neq 0$). For future discussion and comparison with Cluster data, we consider the following numerical values (see section 3.2): temperature $\sim$6 keV leading to a sound speed of $\sim$1000 km/s, magnetic field in the lobe of 28 nT, and a density in the neutral sheet about 0.5 cm^{-3}. The density measured in the plasma sheet boundary layer (PSBL) is about 0.05 cm^{-3} and certainly much smaller in the lobe. As Cluster does not provide a precise value of ρ_e, we choose the usually accepted value [*Lui*, 1987] of about 0.01 cm^{-3}. Thus the ratio ρ_0/ρ_e is close to 50, which is compatible with a pressure equilibrium of the plasma sheet. Its exact value is nevertheless not crucial for the simple temporal analysis performed here. Finally, the spatial quantities are normalized to the half-width a of the sheet.

[14] Figure 2a represents the dispersion curves for the two first eigenmodes in the case of parallel propagation and Figure 2b shows their corresponding spatial structure. The wave number is normalized to a^{-1} and the frequency is normalized to v_s/a. The dispersion relations correspond to almost parallel lines with a typical slope of the order of the sound speed. At small k, they intersect the $\omega = k_x v_{Ae}$ line, whose slope depends on the ratio ρ_0/ρ_e. For a given phase speed $v_\varphi = \omega/k$, there is an infinite set of eigenvalues and eigenfunctions, with an increasing number of nodes, as the standard Sturm-Liouville theory predicts it. For a given wave number, the number of poles is finite and limited by $k_x v_{Ae}$. The frequency gap between two successive solutions is of the order of v_s/a.

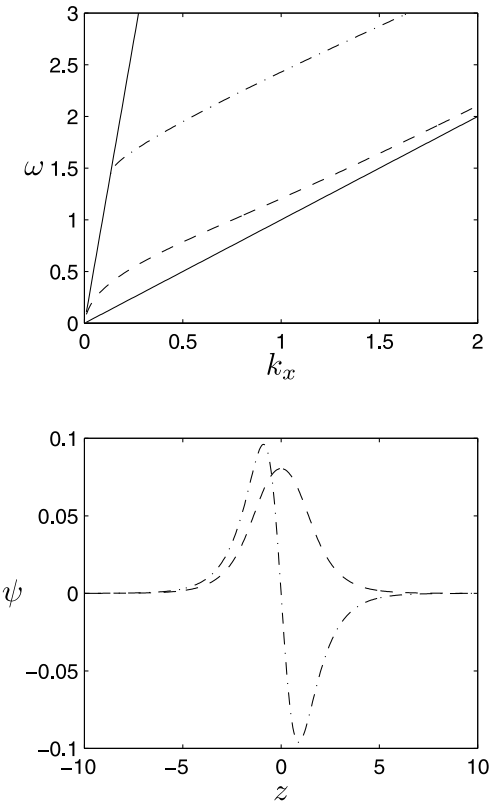

Figure 2. Dispersion relations (a: upper) and eigenfunctions (b: below) for a pure k_x propagation. The dashed line represents the fundamental kink mode and dotted-dashed line the first harmonic sausage mode. The two solid lines on the dispersion diagram correspond to a phase velocity equal to the sound speed and the Alfven speed in the lobes, respectively.

[15] Figure 3 displays the dispersion curves for $k_x = 0$ with the same format as Figure 2. It shows almost the same pattern as before excepted that the fundamental mode merges with the $\omega = k_y v_s$ line.

[16] These dispersion diagrams constitute the basis of our investigation. In the next sections, we indeed use the four Cluster spacecraft to determine the characteristic spatial (a) and temporal (τ) scales of the MHD eigenmodes and compare them to the typical scale of the observed fluctuations.

3. Plasma Sheet Structure and Activity on 22 August 2001

3.1. Overview of the Event

[17] Our choice of the event occurring on 22 August 2001 is motivated by the fact that the sheet was first quiet then active during its crossing by Cluster. Interestingly, different

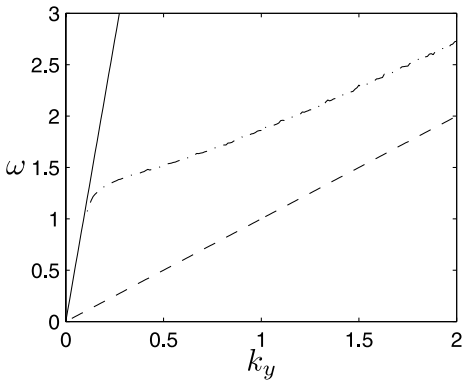

Figure 3. Dispersion relations for the two first modes in the case of a pure k_y propagation. The dashed line represents the fundamental (kink) mode and the dotted-dashed line the first harmonic (sausage) mode. The solid line corresponds to a phase velocity equal to $\sqrt{v_{Ae}^2 + v_s^2}$.

types of perturbations were observed depending on the state of magnetospheric activity.

[18] An overview of the observations made by spacecraft 1 from 0700 to 1200 UT is presented in Figure 4. Starting from the upper panel, we display: (1) the ion energy-time spectrograms from 100 eV to 40 keV measured by CIS-CODIF (see *Rème et al.* [2001] for a description of the CIS experiment), (2) the ion density, (3) the ion temperature, (4) the ion fluid velocity, and (5) the magnetic field (see *Balogh et al.* [2001] for a description of FGM experiment). From a simple inspection of these data, one deduces that Cluster is close to or in the PSBL from 0700 to 0800 UT. The crossing of the sheet itself is performed from ~0800 to ~1115 UT, at $X_{gse} \simeq -18.7$ Earth radius (R_E) in the morning side of the sheet ($Y_{gse} \simeq -3.6\ R_E$), with Z_{gse} varying from ~0.8 R_E to $-2\ R_E$. After 1115 UT, the four spacecraft begin to cross the southern lobe of the tail.

[19] Ground-based magnetic data (not displayed here) show that the magnetosphere is first quiet from 0800 to

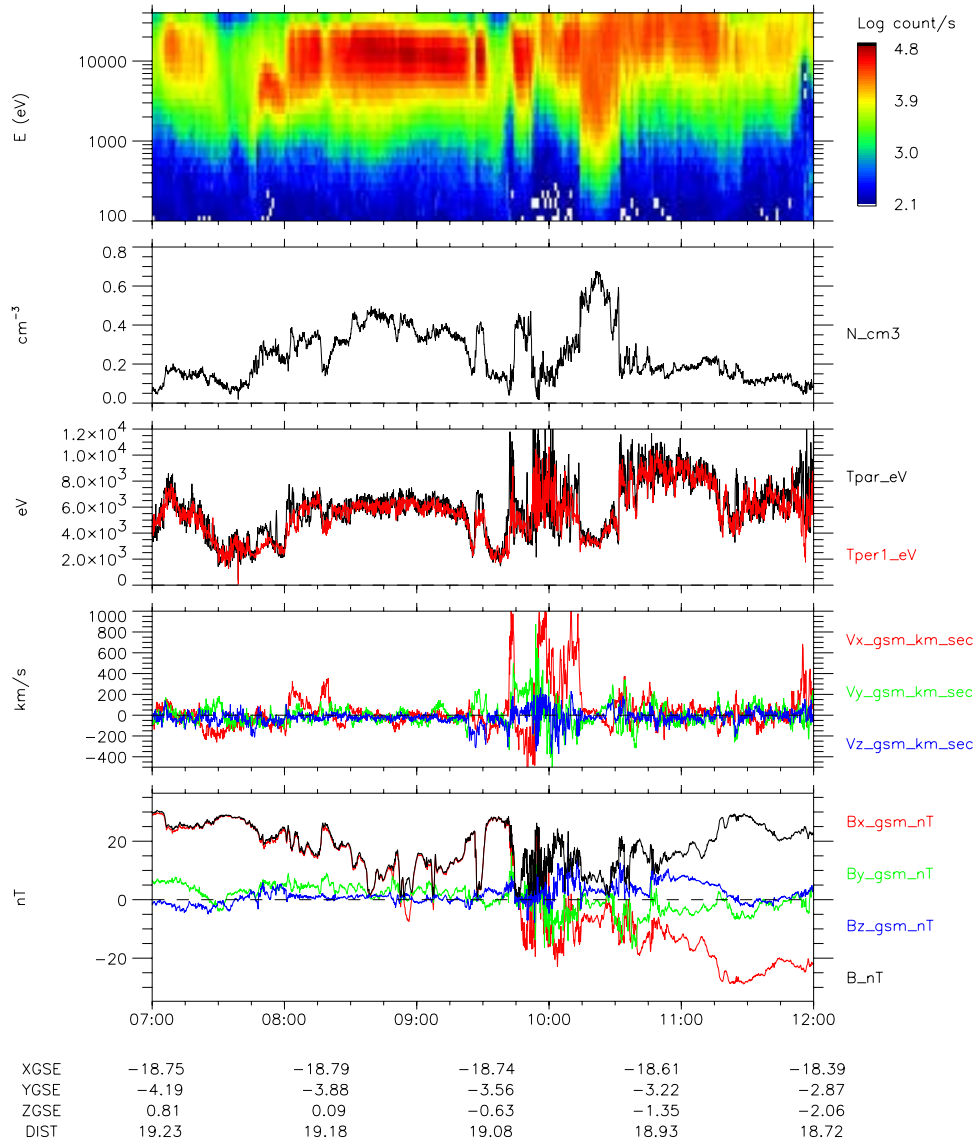

Figure 4. Overview of the 22 August 2001 event. Panel (1): ion energy spectrogram, Panel (2): ion density, Panel (3): temperature, Panel (4): velocity, Panel (5): magnetic field measured by SC1.

0930 UT and significantly more active after 0930 UT. A first manifestation of activity takes place at about 0926 UT likely as a pseudobreakup. Later, a major substorm develops prior to 0940 UT with onset at ~0937 UT. The activity then persists during the whole crossing of the sheet. In particular, a strong intensification occurs at 0940 UT as seen by the Canadian Auroral Network for the OPEN Program Unified Study (CANOPUS) network and the GOES 10 spacecraft.

[20] Large amplitude magnetic fluctuations (larger than 10 nT) are observed during the whole crossing of the sheet. Even at the low time resolution used in Figure 4, fluctuations with rather different characteristics are clearly observed depending on the state of activity. During the quiet period, the fluctuations have typical temporal scales of a few minutes. In a very contrasted way, large-amplitude waves with periods smaller than 1 minute appear around 0940 UT, precisely in conjunction with the development of the magnetospheric activity. These short-period and long-period fluctuations have likely different origins and their identification as specific propagative modes of the sheet deserves a careful analysis. Before considering more sophisticated physical model, a first approach is to examine if the MHD theory developed in section 2 can describe at least a part of the observations. This analysis requires the determination of the MHD parameters of the sheet as well as a relatively precise knowledge of its geometrical structure and in particular its thickness.

3.2. Physical Properties of the Sheet

[21] The density (panel 2) varies from ~0.05 cm^{-3} in the PSBL to 0.4–0.45 cm^{-3} in the central sheet (from 0800 to 0930 UT) with higher values around 1020 UT (~0.6 cm^{-3}). Only particles with energies above 30 eV are taken into account here. The total plasma density can be estimated from the plasma frequency measured by the WHISPER experiment [*Decréau et al.*, 1997]. Around 0800 UT, it is almost 30% larger than the one obtained from CIS. This could indicate that a low-energy plasma, not precisely measured by CIS, is also present in the sheet. In the following, we will assume that a density of 0.5 cm^{-3} in the central sheet and a ratio of 50 with the density in the lobes are reasonable. This ratio is an important parameters of the MHD model since it determines the ratio v_{Ae}/v_s and thus the shape of the domains in the dispersion diagram where localized modes exist ($k_x v_s < \omega < k_x v_{Ae}$). When this ratio is increased, the harmonics can be extended towards lower frequencies (see Figure 2). This ratio thus determines the minimal frequency of a given harmonic in normalized variables.

[22] The temperature (panel 3) in the sheet is about 6 keV before 0930 UT. It then reaches 8 keV around 1000 UT. The corresponding sound velocity would thus be of the order of 1000 km/s. Let us note that from 0800 to 0930 UT, the temperature is almost constant although the spacecraft makes large incursions in the sheet and even reaches the neutral sheet around 0900 UT. This indicates that the use of an isothermal model is adequate. The temperature presents larger variations during the active period. In particular, it raises up to 8 keV around 1000 UT corresponding to a sound speed of the order of 900–1100 km/s.

[23] Earthward flows with velocity larger than 150 km/s are observed as Cluster crosses the PSBL at ~0800–0810 UT (panel 3). Flows with much larger velocities (above 600 km/s) are measured from 0950 to 1015 UT, with also a short burst at 0940 UT. They are observed close to the central sheet sometimes in conjunction with enhancements of the Z magnetic component (from 1000 to 1015 UT) which is characteristic of bursty bulk flows (BBF). At the exception of these periods of large flows that will be not discussed in the present and the companion papers, the possible doppler shift of the observed fluctuations is negligible.

[24] The magnetic field magnitude is ~28 nT at maximum. Assuming a density of ~0.01 cm^{-3} in the lobe, the Alfven velocity will thus be of the order of 6000 km/s. Before 0930 UT, the Z component is almost null (smaller than 2 nT) and the X component is always dominant. This situation is consistent with the use of the 1-D Harris sheet model. After 0930 UT, the situation is more complex. A static Z-component reaching 3 nT is observed from 0930 to 0940 UT. Large oscillations are observed from 0940 to 1000 UT, but in average the Z component is almost null. Then, a static Z component as large as 10 nT is measured after 1005 and after 1045 UT which can be interpreted as an effect of the dipolarization that follows the substorm. Some of the B_z increasing can be related to the occurrence of BBF. We will not comment on this particular aspect of the dynamics of the plasma sheet to concentrate ourselves on the analysis of the wave-like fluctuations. At the exception of some limited time periods, the B_z component is then less than 2–3 nT in average from 0800 to 1030 UT, which legitimates the use of a Harris sheet model, at least for studying modes that are not too strongly affected by a small z component. We also note that the ion gyroperiod (2 s) and the thermal ion gyroradius (~300 km) relative to the magnetic field in the lobe are such that it is a priori reasonable to consider the MHD theory for oscillations with period of a few 10 s propagating in a sheet with thickness larger than typically 2000 km.

4. Identification of MHD Eigenmodes

4.1. Temporal and Spatial Parameters of the Sheet

[25] The relative positions of the spacecraft are shown in Figure 5. The interspacecraft distance is about 2000 km. Considering a sheet with a static field mainly in the X direction, the spacecraft 1 and 4 would be located on very close field lines, at distance smaller than 400 km in the Y/Z plane. Spacecraft 2 would be above the couple (1, 4), in the positive Y direction, and spacecraft 3 would be below the couple (1, 4), also in the positive Y direction. For a 1-D sheet oriented in the nominal direction, with a current in the Y direction, the B_x component is thus expected to be the largest for spacecraft 2 and the smallest for spacecraft 3.

[26] As seen in the upper panel of Figure 6, where the B_x component measured by the four spacecraft is displayed, the situation is more complex. As expected for the crossing of a current layer oriented in the Y direction, spacecraft 3 (in green) systematically measures the smallest B_x component. Nevertheless, spacecraft 4 (in blue) often measures the largest field. This suggests that the sheet is significantly tilted in the Y/Z plane. This tilt as well as the thickness of the sheet can be estimated from a measurement of the magnetic gradient. They are determined by solving the

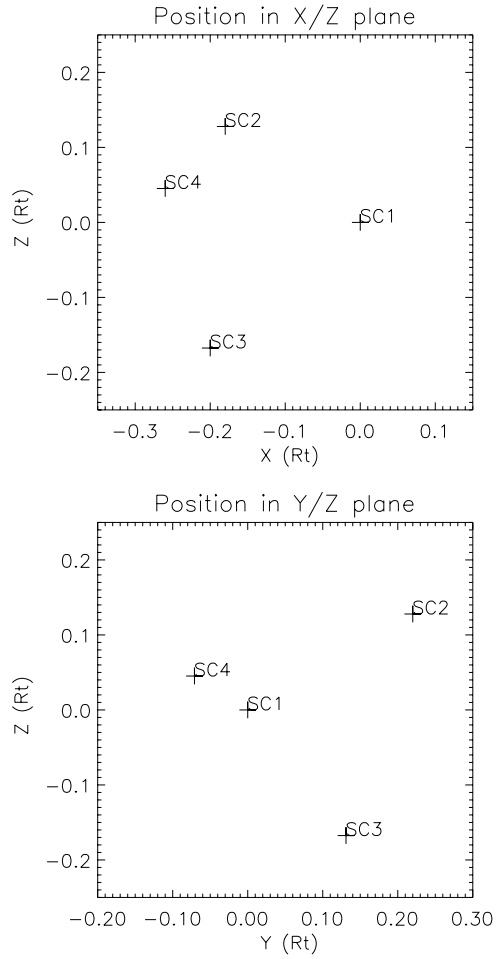

Figure 5. Relative position of the four spacecrafts in the GSM frame.

system of equations obtained from a first order expansion of the magnetic field. Writing

$$B_{x,i} - B_{x,1} = A\vec{\xi} \cdot (\vec{r}_i - \vec{r}_1), \tag{9}$$

where $i = 2, 3, 4$ (we choose spacecraft 1 as reference), $\vec{\xi}$ (the normal to the sheet) and A (the magnetic gradient magnitude) can be obtained at any time.

[27] The projections of $\vec{\xi}$ in the Y/Z and the X/Z plane are shown in panels 2 and 3, respectively. To remove short-period fluctuations, we perform a sliding average over 1 min of the magnetic field. In the Y/Z plane the tilt angle can be as large as 30° and correspond to a positive inclination in the direction of positive Y. In the X/Z plane the tilt is smaller in average. The large perturbations observed before 0930 UT correspond to regular large-amplitude oscillation of the tilt angle, mainly observed in the Y/Z direction. This suggests that they could be associated with large oscillations of the sheet propagating in the Y direction This point will be discussed more precisely in section 5. The situation is more confused during the active period. Let us nevertheless note that the tilt angle is relatively constant in the Y/Z plane before 1000 UT. It rapidly varies in the X/Z plane which can suggest that the oscillations correspond to waves propagating in the X direction. The magnetic gradient A scales the spatial variation of the field. It can be used for a first estimate of the thickness of the sheet (a). Assuming that the magnetic field in lobes is B_l, one gets

$$a \simeq \frac{B_l}{A}. \tag{10}$$

B_l is estimated by assuming that the total pressure in the lobe is mainly magnetic and equal to the total (magnetic + thermal) pressure measured by Cluster in the sheet. B_l is presented in panel 4. It is of the order or slightly larger than 30 nT during the quiet period. It decreases to 25 nT around 1000 UT after the substorm onset. Using the relation in equation (10), the thickness of the sheet is estimated and displayed in panel 5 (thick line). We indicate in yellow the periods of time for which we consider that the magnetic field presents a too small variation (less than 2 nT) from one spacecraft to the other to get a reliable estimate of the sheet thickness. Before 0930 UT, the thickness varies from 1 to 2 R_E. From 0930 to 0940 the spacecraft are in the lobes and the thickness of the sheet cannot be estimated properly. From 0940 to 1000 UT, as the activity develops in the sheet and when the large amplitude coherent waves are observed, the sheet becomes as thin as 0.2–0.3 R_E.

[28] Using the sound speed (v_s) also shown in panel 5 (thin line), one may then determine the MHD characteristic time, $\tau = a/v_s$. This timescale is displayed in panel 6. Before 0930 UT, the characteristic time is typically of the order of 6–8 s. From 0940 to 1000 UT, as the sheet is thinner and hotter, it is rather of the order of 2–3 s.

4.2. Temporal and Spatial Scales of the Fluctuations

[29] The normalized spatial variables and time can be deduced from the thickness of the sheet and the MHD characteristic time estimated in last section. Then, assuming that the observed fluctuations are MHD eigenmodes, one may calculate what would be their wavelength and, as explained below, deduce a selection criterium of possible MHD modes.

[30] With Cluster, it is a priori possible to independently measure the wavelengths and the periods of the fluctuations. However, the wavelength of MHD fluctuations with periods of a few 10 s, as observed in the present case, are larger than a few R_E. This is too large to be directly measurable given the relatively small spacecraft separation (2000 km). We thus cannot use this direct method. We propose another investigation that includes the following stages: (1) considering the magnetic and the pressure observations, we first perform a wavelet analysis of the fluctuations and determine the signal repartition in a temporal scalogram. (2) Using the dispersion curve of the fundamental mode and taking into account the measured sheet thickness and MHD characteristic time, we convert the temporal scalogram into a spatial scalogram. We determine the signal repartition in the spatial domain and identify the fluctuations that could correspond to MHD eigenmodes of reasonable wavelengths. Given the position of Cluster at 18 R_E from Earth, one may indeed consider that fluctuations with wavelength that would be larger than 15 R_E are hardly interpretable as freely propagating eigenmodes of the sheet.

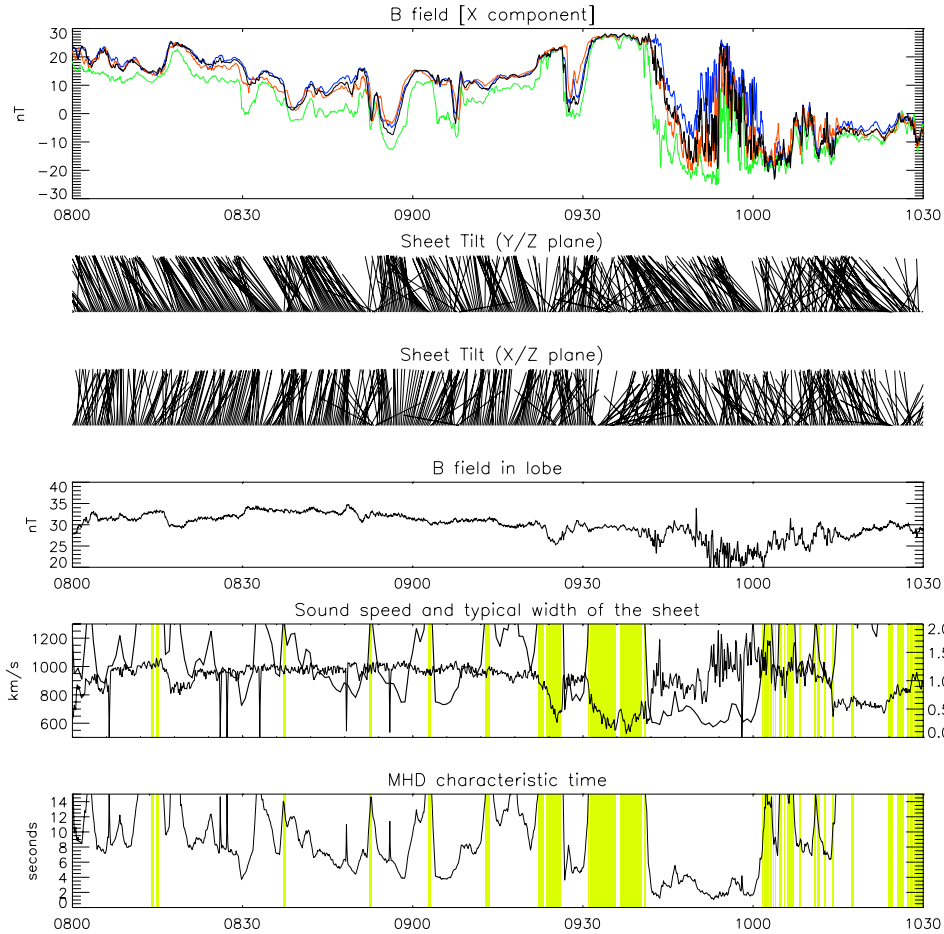

Figure 6. Geometrical and physical parameters of the plasma sheet. Panel 1: B_x component (SC1 in blue, SC2 in red, SC3 in green and SC4 in blue), Panels 2 and 3: projection of the normal vector in plane Y/Z and X/Z, Panel 4: magnetic field in lobe, Panel 5: sound speed and half-thickness of the sheet (thick line), Panel 6: MHD characteristic time $\tau = a/v_s$. The yellow zones correspond to periods of poor estimates of the sheet thickness (Cluster in the lobes).

[31] The results of this investigation are displayed in Figure 7 for the period 0800–1030 UT. On the upper panel, the B_x component measured by spacecraft 4 and its wavelet analysis are shown. We use Morlet's test functions. The analysis is made for periods ranging from 1200 s to 4 s. Below, we show the transposition in the spatial domain. We assume here that the fluctuations are MHD fundamental eigenmodes (kink-like fluctuations) propagating in the X direction. We thus consider the dispersion curve of the fundamental mode displayed in Figure 2. Let us however notice that the final result does not strongly depend on the assumed direction of propagation since the fundamental is in any cases close to the $\omega = kv_s$ line (see Figures 2 and 3). During the quiet period [0800, 0930], large period fluctuations with typical temporal scale larger than 100–150 s dominate. When transposed in the spatial domain, these fluctuations correspond to eigenmodes with typical wavelength larger than 10–20 R_E. There are nevertheless some evidences of fluctuation of shorter scales, for example before 0820 UT and at ~0850 UT. The situation radically evolves during the active period (after 0940 UT). In the time domain, significant amplitudes are observed down to periods of 15 s from ~0940 UT to ~1015 UT. When transposed in the spatial domain, these higher-frequency fluctuations correspond to a strong signal at wavelength smaller than 5 R_E. Significant amplitudes can even be observed at scales of a fraction of R_E. In panels 3 and 4 the same analysis is performed for the pressure. We use here the pressure measured with a 4 s resolution on board spacecraft 4. The results are similar to those obtained from the magnetic field. If interpreted in terms of MHD eigenmodes, the fluctuations observed during the quiet period would again have wavelength larger than 10–20 R_E. By contrast, strong signals (~0.1 nPa) are observed at wavelengths smaller than 5 R_E after ~0950 UT.

[32] In panels 2 and 4 we present the energy repartition in absolute spatial scale. It is also possible to examine this energy repartition relatively to the thickness of the sheet. This is presented in the lowermost panel of the figure where the total amplitudes of magnetic and pressure fluctuations that would have wavelengths smaller than 10 times the sheet half-thickness are displayed. This quantity is obtained by integrating the signal displayed in the spatial scalogram at scales smaller than 10 a. It again clearly appears that it is only after 0950 UT that the

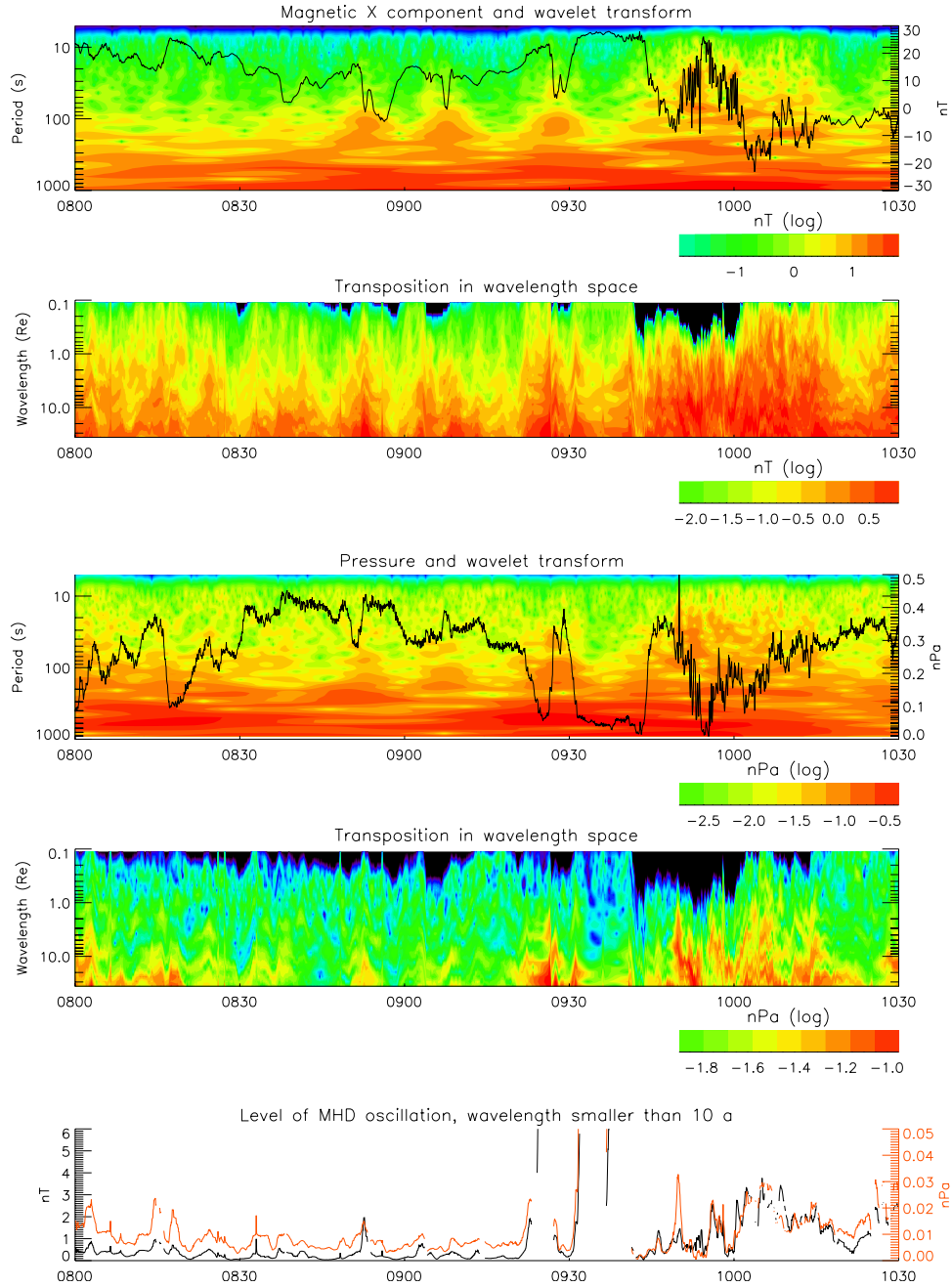

Figure 7. Spatial and temporal scalograms. Panels 1 and 2: temporal and reconstructed spatial scalograms for the magnetic fluctuations, Panel 3 and 4: same quantities for the pressure fluctuations, Pane 5: integrated amplitude of fluctuations at scales smaller than 10*a*.

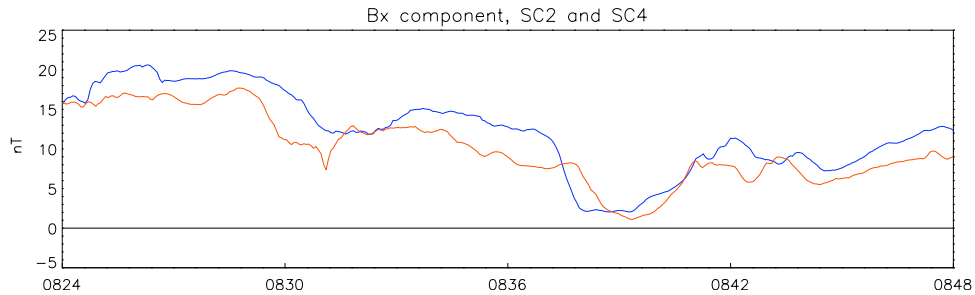

Figure 8. Long period oscillations. The magnetic *X* component is plotted for SC2 (in red) and SC4 (in blue).

energy at these small scales significantly increases. Note that the sharp peaks observed around 0930 are artifacts due to unreliable determinations of the sheet thickness.

5. Discussion and Conclusion

[33] From the analysis performed in the last section we clearly identify two types of oscillations: (1) long period fluctuations observed during the quiet magnetospheric period that would have wavelength larger than typically 15 R_E and (2) shorter period fluctuations observed after the substorm onset with wavelength smaller than 5 R_E.

[34] Let us first discuss the possible nature of the large period fluctuations during the quiet period and their interpretation in terms of MHD oscillations. Their typical timescale is of the order of 150 s which is, as already discussed, not compatible with MHD eigenmodes freely propagating in the X direction. Nevertheless, another possibility could be that they propagate in the Y direction. Considering the fundamental eigenmode propagating in the Y direction (Figure 3), we indeed obtain a wavelength of the order of 19 R_E (for a sound speed of 1000 km/s and a period of 150 s) which is of the order of the Y extension of the sheet for $X \sim -20$ R_E. Although this interpretation is theoretically possible, it presents some difficulties if one considers the correlations between spacecrafts.

[35] The phase and the group velocities of the MHD eigenmodes are indeed close to the sound speed (1000 km/s). Given the spacecraft position, this means that a time delay of 1–2 s at most could be measured from one spacecraft to the other. In Figure 8 we present the B_x component measured by SC2 and SC4 for the period 0824–0848 UT. These two spacecraft are the most distant in the Y direction (see Figure 5). It is clearly seen that the large-scale perturbations slowly propagate in the Y direction. The propagation is negative at 0831 and positive at 0838 with typical velocities of −30 km/s and +60 km/s, respectively (delays of ~ -60 s and $\sim$30 s). These are far below characteristic MHD velocities, so we conclude that these fluctuations cannot be interpreted as a superposition of MHD modes. This also excludes the possibility of stationary waves that would lead to a perfect correlation, without delay, from one spacecraft to the other. To remain in the framework of the ideal MHD, one possibility could be that these oscillations belong to the continuum domain (crosshatched in Figure 1). They would thus propagate at the local cusp or Alfven velocities, both being very small near the neutral sheet. A last possibility is that more complex boundary conditions (in the Y direction or near Earth) than taken into account here have to be considered. This will be studied in future works.

[36] To conclude, we show that only the shortest period (less than 30 s here) fluctuations can easily be interpreted as MHD eigenmodes. They are indeed compatible with the fundamental mode. They would have relatively short wavelength, of the order of or less than 5–6 R_E. These short-scale fluctuations will be studied into more details in the companion paper *Fruit et al.* [2004], where it will be shown that they are partly a superposition of kink-like and sausage-like MHD eigenmodes propagating in the X direction, that may have been excited by a vertical displacement of the sheet.

[37] **Acknowledgments.** Lou-Chuang Lee thanks Rudolf A. Treumann and another reviewer for their assistance in evaluating this paper.

References

Balogh, A., et al. (2001), The Cluster magnetic field investigation: Overview of in-flight performance and initial results, *Ann. Geophys.*, *19*, 1207–1217.

Bauer, T. M., W. Baumjohann, and R. A. Treumann (1995a), Neutral sheet oscillations at substorm onset, *J. Geophys. Res.*, *100*, 23,737.

Bauer, T. M., W. Baumjohann, R. A. Treumann, N. Sckopke, and H. Luhr (1995b), Low frequency waves in the near-earth plasma sheet, *J. Geophys. Res.*, *100*, 9605.

Coppi, B., G. Laval, and R. Pellat (1966), Dynamics of the geomagnetic tail, *Phys. Rev. Lett.*, *16*, 1207.

Coroniti, F. V. (1985), Explosive tail reconnection: The growth and expansion phases of magnetospheric substorms, *J. Geophys. Res.*, *90*, 7427.

Dahlburg, R. B., S. K. Antiochos, and T. A. Zang (1992), Secondary instability in three-dimensional magnetic reconnection, *Phys. Fluids*, *B4*, 3902.

Daughton, W. (1998), Kinetic theory of the drift kink instability in current sheet, *J. Geophys. Res.*, *103*, 29,429.

Daughton, W. (2002), Nonlinear dynamics of thin current sheets, *Phys. Plasmas*, *9*, 3668.

Decréau, P. M. E., et al. (1997), Whisper, a resonance sounder and wave analyser: Performances and perspectives for the Cluster mission, *Space Sci. Rev.*, *79*, 157–193.

Fruit, G., P. Louarn, A. Tur, and D. LeQuéau (2002a), On the propagation of magnetohydrodynamic perturbations in a Harris-type current sheet: 1. Propagation on discrete modes and signal reconstruction, *J. Geophys. Res.*, *107*(A11), 1411, doi:10.1029/2001JA009212.

Fruit, G., P. Louarn, A. Tur, and D. LeQuéau (2002b), On the propagation of magnetohydrodynamic perturbations in a Harris-type current sheet: 2. Propagation on continuous modes and resonant absorption, *J. Geophys. Res.*, *107*(A11), 1412, doi:10.1029/2001JA009215.

Fruit, G., et al. (2004), On the propagation of low-frequency fluctuations in the plasma sheet: 2. Characterization of the MHD eigenmodes and physical implications, *J. Geophys. Res.*, *109*, A03217, doi:10.1029/2003JA010229.

Harris, E. G. (1962), On a plasma sheath separating region of oppositely directed magnetic field, *Nuovo Cimento*, *23*, 115.

Huba, J. D., J. F. Drake, and N. T. Gladd (1980), Lower hybrid drift instability in field reversed plasmas, *Phys. Fluids*, *23*, 552.

Kepko, L., and M. Kivelson (1999), Generation of Pi2 pulsations by bursty bulk flows, *J. Geophys. Res.*, *104*, 25,021.

Krall, N. A., and P. C. Liewer (1971), Low frequency instabilities in magnetic pulses, *Phys. Rev. A*, *4*, 2094.

Lapenta, G., and J. U. Brackbill (1997), A kinetic theory for the drift-kink instability, *J. Geophys. Res.*, *102*, 27,099.

Lee, L. C., S. Wang, C. Q. Wei, and B. T. Tsurutani (1988), Streaming sausage, kink and tearing instabilities in a current sheet with application to the Earth's magnetotail, *J. Geophys. Res.*, *93*, 7354.

Lembege, B., and R. Pellat (1982), Stability of a thick two-dimensional quasineutral sheet, *Phys. Fluids*, *52*, 1995.

Lui, A. T. (1987), *Magnetotail Physics*, Johns Hopkins Univ. Press, Baltimore, Md.

Lui, A. T. (1996), Current disruption in the Earth's magnetosphere: Observations and models, *J. Geophys. Res.*, *101*, 13,067.

McKenzie, J. F. (1970), Hydromagnetic oscillations of the global magnetotail and plasma sheet, *J. Geophys. Res.*, *75*, 5331.

Miura, A., S. Ohtani, and T. Tamao (1989), Ballooning instability and structure of diamagnetic waves in a model magnetosphere, *J. Geophys. Res.*, *94*, 15,231.

Patel, V. L. (1968), Magnetospheric tail as a hydromagnetic wave guide, *Phys. Lett.*, *26A*, 596.

Pellat, R., F. V. Coroniti, and P. L. Pritchett (1991), Does ion tearing exist?, *Geophys. Res. Lett.*, *18*, 143.

Pritchett, P. L. (2001), Collisionless magnetic reconnection in a three-dimensional open system, *J. Geophys. Res.*, *106*, 25,961.

Rème, H., et al. (2001), First multispacecraft ion measurements in and near the Earth's magnetosphere with the identical Cluster ion spectrometry (CIS) experiment, *Ann. Geophys.*, *19*, 1303.

Roux, A., et al. (1991), Plasma sheet instability related to the westward traveling surge, *J. Geophys. Res.*, *96*, 17,697.

Schindler, K., and N. F. Ness (1974), Neutral point detection by satellites, *J. Geophys. Res.*, *79*, 5297.

Seboldt, W. (1990), Nonlocal analysis of low-frequency waves in the plasma sheet, *J. Geophys. Res.*, *95*, 10,471.

Siscoe, G. L. (1969), Resonant compressional waves in the geomagnetic tail, *J. Geophys. Res.*, *74*, 6482.

Smith, J. M. B., B. Roberts, and R. Olivier (1997), Magnetoacoustic wave propagation in current sheets, *Astron. Astrophys.*, *327*, 377.

Tirry, W. J., V. M. Cadez, and M. Goossens (1997), MHD surface type quasi-modes of a current sheet model, *Astron. Astrophys.*, *324*, 1170.

Volwerk, M., K. H. Glassmeier, A. Runov, W. Baumjohann, R. Nakamura, T. L. Zhang, B. Klecker, A. Balogh, and H. Rème (2003), Kink mode oscillation of the current sheet, *Geophys. Res. Lett.*, *30*(6), 1320, doi:10.1029/2002GL016467.

A. Balogh and E. Lucek, Imperial College, South Kensington Campus, London SW7 2BZ, UK. (a.balogh@ic.ac.uk; e.lucek@ic.ac.uk)

E. Budnik, C. Jacquey, D. Le Quéau, P. Louarn, H. Rème, and J. A. Sauvaud, Centre d'Etude Spatiale des Rayonnements, 9 avenue du Colonel Roche, BP 4346, 31028 Toulouse cedex 4, France. (budnik@cesr.fr; jacquey@cesr.fr; lequeau@cesr.fr; louarn@cesr.fr; reme@cesr.fr; sauvaud@cesr.fr)

G. Fruit, University of Waikato, Private Bag 3105, Hamilton, New Zealand. (fruit@math.waikato.ac.nz)